

Very Short Term Time-Series Forecasting of Solar Irradiance Without Exogenous Inputs[☆]

Elin Klages^{a,1}, Christian A. Hans^{a,2}

^a*Control Systems Group, Technische Universität Berlin, Germany*

Abstract

This paper compares different forecast methods and models to predict average values of solar irradiance with a sampling time of 15 min over a prediction horizon of up to 3 h. The methods considered only require historic solar irradiance values, the current time and geographical location, i.e., no exogenous inputs are required. Nearest neighbor regression (NNR) and autoregressive integrated moving average (ARIMA) models are tested using different hyperparameters (e.g., the number of autoregressive lags, or the size of the training data set) and data from different locations and seasons. Based on a high number of different models, NNR is identified to be the more promising approach. The hyperparameters and their effect on the forecast quality are analyzed to identify properties which are likely to lead to good forecasts. Using these properties, a reduced search space is derived which can be used to identify good forecast models much faster. In a case study, the use of this search space is demonstrated by finding forecast models for different climatic situations.

Keywords: Solar forecasting, Time-series forecast, Nearest-neighbor regression, ARIMA

1. Introduction

In the last years, the capacity of globally installed photovoltaic generators continuously increased from 6 GW in 2006 to 303 GW in 2016 [1]. With this growth, the intermittent nature of the infeed of photovoltaic power plants became a major challenge in the operation of electric grids [2]. One important part in addressing this challenge is the use of accurate forecasts to predict the infeed of photovoltaic power plants with a high temporal resolution [3].

1.1. Related work

Various studies on short term forecasting of photovoltaic power plant infeed, e.g., [4–8], and solar irradiance, e.g., [9–11], have been published. Autoregressive integrated moving average (ARIMA) models have been widely adopted in this context, e.g., in [4, 7, 9]. Furthermore, in the last decades forecast methods that employ techniques from artificial intelligence have become more prominent. Most of them, e.g., [4, 8–11], use artificial neural networks. Others employ support vector regression, e.g., [6, 8], and nearest neighbor regression (NNR), e.g., [4, 5].

Despite additional effort that comes with the use of exogenous inputs, e.g., cloud cover, air temperature, only in [4, 7, 10] forecasts without exogenous inputs are considered. Another limitation of most existing publications, e.g., [4–7, 10, 11], is that the forecast models are obtained using only one data set. This makes it hard to draw general conclusions from the analysis that could be transferred to other locations or seasons of the year. Moreover, in [4–6, 9–11] the model selection

[☆]This work was partially supported by the German Federal Ministry for Economic Affairs and Energy (BMWi), Project No. 0324024A.

Email addresses: elin.ae.klages@campus.tu-berlin.de (Elin Klages), hans@control.tu-berlin.de (Christian A. Hans)

¹Currently at the Institute of Modelling and Computation, Technical University Hamburg, Germany.

²Corresponding author.

process is not explicitly discussed. Even though high forecast accuracies could be achieved for single data sets, due to the missing description of the selection processes the findings cannot be directly used for different data sets. For example, in [11] the authors state that they used a search and in [9] that they tried different model structures to choose an artificial neural networks. However, they did not provide information on the search space. In [6], a search space for support vector regression forecasts is provided but no information on the selection criterion or the final model structure and parameters is given. The structure of an artificial neural networks forecast model is examined in [10] using a sensitivity analysis. Unfortunately, the publication does not contain sufficient details of the analysis to replicate it on different data. To the knowledge of the authors only in [5] a search space is provided and the results are analyzed to gain information about suitable model structure. Unfortunately, the analysis is only performed on data from one location. This makes it hard to identify a reduced search space and in practice often leads to exhaustive searches and tests to find suitable forecast models.

1.2. Contributions

In this paper we derive a significantly reduced search space that has a high probability of finding a sufficiently accurate forecast model. It is based on conclusions drawn from an exhaustive search using data from three different locations and three different seasons. For every season and location ARIMA and seasonal ARIMA (SARIMA) as well as NNR and seasonal NNR (SNNR) models were trained for different hyperparameters. The forecast accuracy of the different models was then assessed and recommendations for a future hyperparameter search were derived. These include the use of NNR and SNNR over the use of ARIMA and SARIMA as the probability of finding a good NNR or SNNR model is much higher. Furthermore, recommendations regarding the model hyperparameters, e.g., the numbers of historic data points used to train the models or different autoregressive lags, are identified. Also, the handling of night data and the use of transmissivity instead of irradiance is analyzed. Unlike existing work, every step of the model selection process is explained in detail, providing the necessary information to implement a similar search for different data sets. In a numerical case study, this reduced search space is used to find forecast models for distinct climatic situations of an independent data set.

To allow for a simple and robust forecast, this work focuses on predictions of solar irradiance without exogenous inputs, i.e., using only historic irradiance data, time and location. Motivated by the smallest intraday interval of energy trading in Germany the forecast prediction interval was chosen to be 15 min [12]. In order to cover a possible full charge or discharge of small to medium size storage units, forecasts are performed up to 3 h ahead.

1.3. Outline

The remainder of this paper is organized as follows. Solar irradiance and data preprocessing are discussed in Section 2. In Section 3, basics on time-series forecasting and on the evaluation of forecast accuracy are introduced. The forecasting methods considered in this work are presented in Section 4. Then, the model selection procedure including the data used and the hyperparameters considered are discussed in Section 5. In Section 6 the results of the hyperparameters search are analyzed and applied in Section 7 in a case study.

1.4. Preliminaries

Throughout this paper, real numbers are denoted by \mathbb{R} and integers by \mathbb{N} . Positive integers are denoted by $\mathbb{N}_{>0}$ and nonnegative integers by $\mathbb{N}_{\geq 0}$. The transpose of a matrix x is x^T and the euclidean norm of a vector $x \in \mathbb{R}^N$ is $\|x\|_2 = \sqrt{\sum_{i=1}^N x_i^2}$. The sum over all elements of the set $\mathbb{K} \subset \mathbb{N}$ where every element $i \in \mathbb{K}$ is taken exactly once is denoted by $\sum_{i \in \mathbb{K}} x_i$.

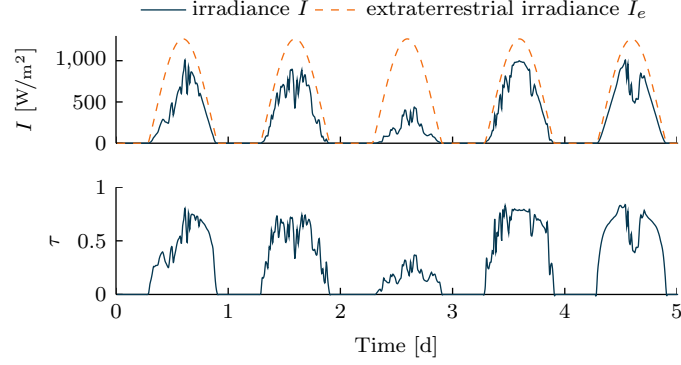


Figure 1: Global horizontal irradiance, extraterrestrial irradiance and the transmissivity over a duration of 5 d. The irradiance values are taken from [15], the extraterrestrial irradiance was estimated using [16].

2. Solar Irradiance

The solar energy that reaches the outer earth's atmosphere is called extraterrestrial solar radiation [13]. It can be estimated employing the information on the energy emitted by and the position of the sun. Ground level solar radiation is more challenging to predict as parts of solar radiation are absorbed, reflected, and scattered by the atmosphere and clouds, [14]. The rate of solar radiation that reaches a horizontal plane on earth per unit area at time $t \in \mathbb{R}_{\geq 0}$, is called global horizontal irradiance $I_t \in \mathbb{R}_{\geq 0}$. The global horizontal irradiance includes the direct normal irradiance, which originates directly from the sun, and the diffuse irradiance, which includes scattered and ground reflected components, [13].

For forecasting, it can be beneficial to normalize the solar irradiance I_t by the extraterrestrial irradiance $I_{e,t} \in \mathbb{R}_{\geq 0}$ (see Figure 1). This yields to transmissivity, [8], also referred to as clearness index, [14], and defined as

$$\tau_t = \frac{I_t}{I_{e,t}}. \quad (1)$$

In this work, the solar position algorithm from [16] is used to estimate the extraterrestrial irradiance $I_e(t)$. This algorithm only requires the position of the surface for which the irradiance shall be determined to calculate the zenith angle $\zeta_t \in [0, 2\pi)$, i.e., the incidence angle of the sun light on a horizontal plane on the earth's surface [17] (see Figure 2). Using ζ_t , the extraterrestrial irradiance can be determined by

$$I_{e,t} = \epsilon_t I_s \cos(\zeta_t), \quad (2)$$

where ϵ_t is a correction factor and $I_s = 1360.8 \text{ W/m}^2$ is the solar constant.

Alternatively, the clear sky index can be used as a normalized time series of irradiance. In this case, the solar irradiance reaching the earth's surface is normalized by the clear sky irradiance, i.e., the irradiance reaching the earth's surface if the sky is without clouds, but reduced by the earth atmosphere. The clear sky index can, for example, be estimated using historic solar irradiance values, [18]. However, due to a lack of historic clear sky irradiance data, we decided to use the clearness index and employ solar position algorithm from [16] to estimate $I_{e,t}$.

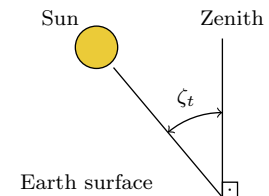


Figure 2: Zenith angle ζ_t to describe the position of the sun at time t .

3. Time-Series Forecasting

In this section, some basics of time-series forecasting are introduced. Also, the evaluation of the forecast accuracy is discussed.

A time series is a collection of $n \in \mathbb{N}_{>0}$ chronologically ordered observations y_1, y_2, \dots, y_n . In this collection, every element y_t refers to an observation performed at a time instant $t = 1, \dots, n$. Time-series forecasting refers to using some of these elements to forecast future data points of a time series, [19]. Forecasts can be univariate or multivariate. Univariate forecasts consider only historic data from one time series of interest. Multivariate forecasts consider multiple time series to forecast one time series. In this work, only univariate forecasts, i.e., forecasts using only historic irradiance to forecast future irradiance, have been considered. Thus, in the following all elements $y_t \in \mathbb{R}$ for $t = 1, \dots, n$ are real-valued scalars.

Broadly speaking, a forecasting method is a procedure to estimate future values $\hat{y}_{t+j|t}$ of a time series based on past values Y_t , i.e.,

$$\hat{y}_{t+j|t} = f(Y_t). \quad (3)$$

Here, $Y_t \in \mathbb{R}^n$ refers to the independent variable. In case of univariate forecasting, the independent variable only includes the present and past values of the time series being forecast, i.e.,

$$Y_t = [y_t \quad y_{t-1} \quad \dots \quad y_{t-n+1}]^T \quad (4)$$

where $n \in \mathbb{N}_{>0}$ is the number of elements in x_t . The forecast time series value $\hat{y}_{t+j|t}$ is the dependent variable. The first index $t + j$ refers to the forecast time instant with prediction step $j \in \mathbb{N}_{>0}$. The second index t refers to the last known value, used to forecast $\hat{y}_{t+j|t}$.

The vector Y_t can also be based on non-consecutive lags, e.g., to represent seasonal behavior. An example for such a vector is

$$Y_t = [y_t \quad y_{t-s+1} \quad y_{t-s}]^T, \quad (5)$$

where $s \in \mathbb{N}_{>0}$ is the length of the season, e.g., one day. In this example, the present observation, y_t , the observation from the last day, y_{t-s+1} , at the same time as the predicted value, \hat{y}_{t+1} , and the observation from the previous day (current time minus 24 h), y_{t-s} , are included.

3.1. Multiple-Step Forecasts

To create multiple step ahead forecasts, a recursive strategy can be applied (see, e.g., [20, Section 4.]). The forecasting model is used for the one step forecasts, where the elements of Y_t are adapted at each step until prediction step $J \in \mathbb{N}_{>0}$ is reached. For example, if Y_t includes the last three data points, $Y_t = [y_t \quad y_{t-1} \quad y_{t-2}]^T$ then the procedure for $J = 12$ prediction steps would be

$$\hat{y}_{t+1|t} = f(Y_t) = f([y_t \quad y_{t-1} \quad y_{t-2}]^T), \quad (6a)$$

$$\hat{y}_{t+2|t} = f(\hat{Y}_{t+1|t}) = f([\hat{y}_{t+1|t} \quad y_t \quad y_{t-1}]^T), \quad (6b)$$

$$\vdots$$

$$\hat{y}_{t+12|t} = f(\hat{Y}_{t+11|t}) = f([\hat{y}_{t+11|t} \quad \hat{y}_{t+10|t} \quad \hat{y}_{t+9|t}]^T). \quad (6c)$$

For seasonal models, the vector $\hat{Y}_{t+j|t} \in \mathbb{R}^n$ for $j \in \mathbb{N}_{>0}$ is adapted at each step in a similar manner by replacing historic data by previous forecast values.

3.2. Evaluation of Forecast Accuracy

To compare the forecast accuracy of different models used for different data sets, some basics need to be discussed. First, the handling of night data is illustrated in this section. Then, the root mean square error is introduced.

3.2.1. Handling of Night Data

Forecasts of data points during night, i.e., of zero irradiance values, were not included in the evaluation of the forecast accuracy. Therefore, observations with a zenith angle

$$\zeta_t \leq 90.83^\circ \quad (7)$$

were excluded based on [21]. In those cases, where ζ_t was not included in the data set it was estimated using [16].

3.2.2. Root Mean Square Error (RMSE)

To determine the quality of a forecast, the root mean square error (RMSE) is calculated separately for every prediction step. Assuming that $m \in \mathbb{N}_{>0}$ forecasts over a prediction horizon of J were performed, the RMSE for prediction step $j = 1, \dots, J$ is

$$e_j = \sqrt{\frac{1}{m} \sum_{t=1}^m (\hat{y}_{t+j|t} - y_{t+j})^2}. \quad (8)$$

This way, the accuracy achieved for the different prediction steps, can be analyzed separately. In the model section process in Section 6, the forecast accuracy of each model on each test data set was compared to the forecast accuracy of a persistence model on the same data, as proposed by [22].

4. Forecasting Methods

This section presents the different forecasting methods employed in this work. First, the persistence model that was used as reference is presented. Then, ARIMA models and nearest neighbor regression are introduced.

4.1. Persistence Models

The basic idea of the persistence model, also called naive model, is that future values are equal to known past values. In this work, the model, $\hat{y}_{t+1|t} = y_t$ is used. However, it is also possible to consider a seasonal persistence model using, e.g., data from the previous day, week or year. This can be described by $\hat{y}_{t+m|t} = y_{t+m-s}$ where $s \in \mathbb{N}_{>0}$ is the seasonal period and $m \in \mathbb{N}_{>0}$ is the forecasting time instant.

4.2. Autoregressive Integrated Moving Average (ARIMA) Models

ARIMA models are widely used for time-series forecasting. Future values are estimated using a linear combination of previously observed values and forecasting errors. Also, differencing can be applied to obtain stationary data. An ARIMA model can be described by (see [23])

$$\Phi(B)\nabla^d y_k = \theta_0 + \Theta(B)e_t, \quad (9)$$

where B is the backwards shift operator with $B^m y_t = y_{t-m}$, and ∇ is the backwards difference operator with $\nabla^d y_t = (y_t - y_{t-1})^d$, $d \in \mathbb{N}_{\geq 0}$. Furthermore, $\Phi(B)$ is the autoregressive part, ∇^d the integrative part, $\Theta(B)$ the moving average part, and e_t is the error of the forecast compared to the measured value. The autoregressive and the moving average operator are polynomials of the form,

$$\Phi(B) = 1 - \phi_1 B^1 - \phi_2 B^2 - \dots - \phi_p B^p, \quad (10)$$

$$\Theta(B) = 1 - \theta_1 B^1 - \theta_2 B^2 - \dots - \theta_q B^q, \quad (11)$$

with $\phi_1, \dots, \phi_p \in \mathbb{R}$, $\theta_1, \dots, \theta_q \in \mathbb{R}$ and $p, q \in \mathbb{N}$.

To fit a model to data that exhibits seasonality, ARIMA models can be extended by seasonality of period $s \in \mathbb{N}_{>0}$. These, so called SARIMA models, can be described by,

$$\Phi(B)\Phi(B)\nabla^d \nabla_s^D y_t = \theta_0 + \Theta(B)\Theta(B)e_t, \quad (12)$$

where $\Phi(B)$ and $\Theta(B)$ are the seasonal autoregressive and seasonal moving average part, defined as

$$\Phi(B) = 1 - \Phi_1 B^s - \Phi_2 B^{2s} - \dots - \Phi_P B^{Ps}, \quad (13)$$

$$\Theta(B) = 1 - \Theta_1 B^s - \Theta_2 B^{2s} - \dots - \Theta_Q B^{Qs}, \quad (14)$$

with $\Phi_1, \dots, \Phi_P \in \mathbb{R}$, $\Theta_1, \dots, \Theta_Q \in \mathbb{R}$ and $P, Q \in \mathbb{N}$, and ∇_s^D represents seasonal differencing

$$\nabla_s^D y_t = (y_t - y_{t-s})^D. \quad (15)$$

For the implementation of the ARIMA models, the econometrics toolbox in MATLAB 2015b, [24], was used. Within the toolbox, maximum likelihood estimation is applied to provide estimates of the model parameters.

4.3. Nearest Neighbor Regression (NNR)

In the following based on [25], we introduce NNR. In NNR the current pattern of historic data, $Y_t \in \mathbb{R}^n$, is compared to previous patterns $Y_i \in \mathbb{R}^n$, $i = 0, \dots, N-1$ in the reference sample $\mathbb{D} \subset \mathbb{R}^n \times \mathbb{R}$ to forecast \hat{y}_t . Broadly speaking, the reference sample is a set, composed of historic data points, i.e.,

$$\mathbb{D} = \{(Y_0, y_1), (Y_1, y_2), \dots, (Y_{N-1}, y_N)\}, \quad N \in \mathbb{N}_{>0},$$

Although NNR allows to use arbitrary elements in Y_i , e.g., $Y_i = [y_{i-13} \ y_{i-111} \ y_{i-2678}]^T$, we follow the notion of autoregressive and seasonal autoregressive lags of (seasonal) ARIMA models to enable a comparison of both methods. For NNR this means that according to the number autoregressive lags p the vectors Y_i in \mathbb{D} are formed. Thus, analog to ARIMA models the entries of the NNR reference sample with $p = 3$ autoregressive lags would have the form

$$Y_i = [y_i \ y_{i-1} \ y_{i-2}]^T \quad (16)$$

The same holds for the seasonal autoregressive lags. In a similar fashion as in (12), the seasonal autoregressive part is multiplied with the autoregressive part. Thus, analog to SARIMA models an NNR reference sample with $p = 3$ autoregressive lags, $P = 2$ seasonal autoregressive lags and a season of $s = 10$ would lead to entries

$$Y_i = [y_i \ y_{i-1} \ y_{i-2} \mid y_{i-9} \ y_{i-10} \ y_{i-11} \ y_{i-12} \mid y_{i-19} \ y_{i-20} \ y_{i-21} \ y_{i-22}]^T. \quad (17)$$

Analog to the SARIMA models, the elements of the previous seasons that correspond to the forecast $\hat{y}_{i+1|i}$, here y_{i-9} and y_{i-19} , are included in the historic data Y_i . Note that this is caused by the zero order term, i.e., the 1, that the polynomials (10) and (13) start with.

A forecasting model, i.e., a regression function to derive a forecast, can be obtained using the $k \in \mathbb{N}_{>0}$ elements in \mathbb{D} that have the smallest distance to Y_t . By defining the set of k nearest neighbors of Y_t as $\mathbb{K}(Y_t) \subseteq \mathbb{D}$, the forecast model can be written as

$$\hat{y}_{t+1|t} = f(Y_t, \mathbb{D}) = \frac{1}{k} \sum_{Y_i \in \mathbb{K}(Y_t)} y_{i+1}. \quad (18)$$

Note that the number of neighbors k can be a fixed number or determined by maximum distance $\varepsilon \in \mathbb{R}_{>0}$. In this work, the euclidean norm is applied to measure the distance between two vectors Y_i and Y_j , $i, j \in \mathbb{N}_{>0}$, i.e.,

$$d(Y_i, Y_j) = \|Y_i - Y_j\|_2. \quad (19)$$

Thus, the set of neighbors closer than ε to Y_t is given by $\mathbb{K}(Y_t) = \{Y_i \in \mathbb{D} \mid d(Y_i, Y_t) \leq \varepsilon\}$.

The model defined in (18), can be modified using a weighted average. In this work, weights inverse to the distance between x_t and the neighbor x_i , have been used, i.e.,

$$\hat{y}_{t+1|t} = f(Y_t, \mathbb{D}) = \begin{cases} \frac{1}{k} \sum_{Y_i \in \mathbb{K}(Y_t)} \frac{1}{d(Y_i, Y_t)} y_{i+1}, & \text{if } d(Y_i, Y_t) \neq 0 \ \forall Y_i \in \mathbb{K}(Y_t), \\ y_{t+1}, & \text{if } \exists Y_l \in \mathbb{K}(Y_t) \text{ with } d(Y_t, Y_l) = 0. \end{cases} \quad (20)$$

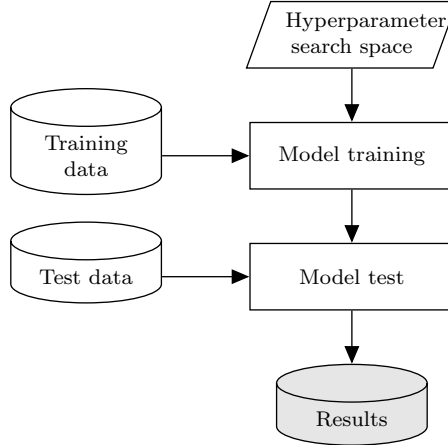


Figure 3: Scheme used to obtain data on forecast accuracy for different models.

Although, (18) requires no training, in the following, the model and the selected reference sample will be referred to as trained model, to increase readability. Instead of training a model using historic data, in NNR the data is used directly in form of the reference sample. Therefore, the reference sample for NNR has a similar meaning as the parameters of trained SARIMA models.

For implementation, the Statistical Learning Toolbox for MATLAB [26] was used. For this work, we used approximated nearest neighbors, a faster algorithm than the exhaustive search for the nearest neighbors, which is also part of the toolbox. Although, it is not guaranteed that the actual nearest neighbor is found, a comparison of the exact and the approximate nearest neighbor search using the data described in Section 5.1 showed no significant difference regarding the forecast accuracy.

5. Hyperparameter Search

We aim to compare the forecast accuracy for different forecast model structures and different sets of historic data used for training. Therefore, an exhaustive search has been performed for each forecasting method to evaluate what kind of models approximate most accurately the test data. To uniquely describe the different model structures and sets of historic data, hyperparameters are used. In the performed hyperparameter search, different model structures are trained using different sets of historic data. Moving along Figure 3, in this section first the time series data used to train and test different forecast models will be introduced. Then, the hyperparameter search space considered will be discussed. Finally, the training and the test of the different models will be illustrated.

5.1. Training and Test Data

For training and testing data sets from three locations, provided by the National Renewable Energy Laboratory (NREL) [27, 28] and by the Atmospheric Radiation Measurement (ARM) Climate Research Facility [15] were used. From these data sets three different seasons were selected to include different climatic situations in the hyperparameter search and thus allow for more general conclusions in the analysis. For every location and every season (i.e., for 9 data sets) the observations were divided into training data (up to 2 months) and independent test data (1 week) that is not used for training.

For testing, data of one week, always following directly the data used for training, was employed (see Figure 4). At each possible data point, the next 3 h, i.e., $J = 12$ future values were predicted. To assure that each model is evaluated based on the forecasts of the same data points, the required historic data to forecast the first data point of the test data set for every model, was also added to the specific test data for each model. As can be observed in Figure 4, the nine selected weeks include different sequences of irradiance, e.g., a sunny week in December from the NREL Clark Station, a

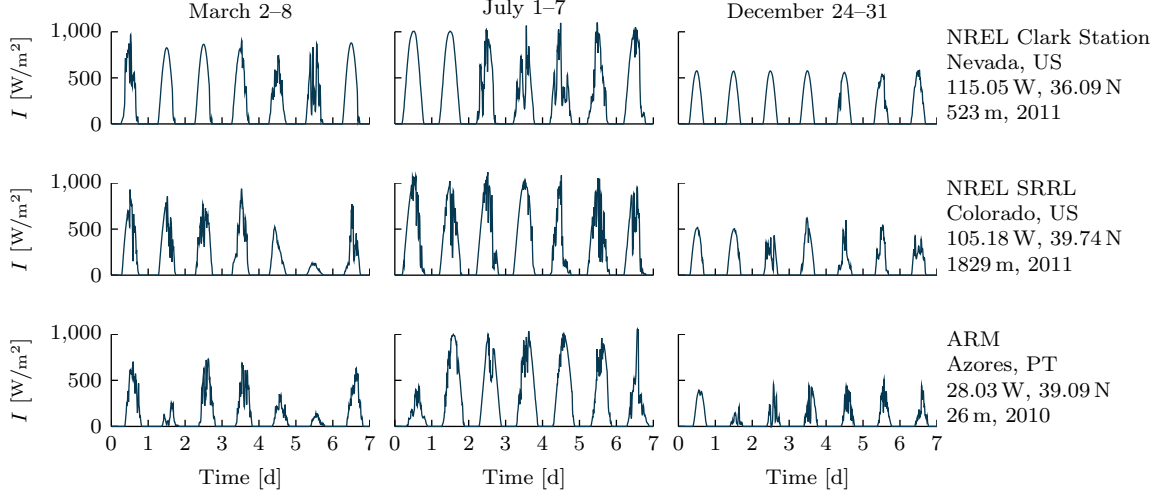


Figure 4: Measured solar irradiance from different geographical locations and different seasons used to test the trained models.

cloudy week in March from the ARM Facility, and various weeks with a combination of sunny, foggy and cloudy days.

5.1.1. Decimation

All of the data sets that were considered have a resolution of 1 min. As a lower temporal resolution was considered more practically relevant, the 15 min average values y_1, y_2, \dots, y_N were derived from the original time series $y'_1, y'_2, \dots, y'_{15N}$ using

$$y_t = \frac{1}{15} \sum_{q=1}^{15} y'_{q+15(t-1)}. \quad (21)$$

5.2. Hyperparameters

The hyperparameters considered can be divided into those that describe the set of historic data and those that describe the model structure used. In the following, both will be discussed.

5.2.1. Data Hyperparameters

The hyperparameters concerning the data used to train the different forecast models is independent of the forecasting method and the model structure considered. As illustrated in this section, we considered modifications of training data by pre- and postprocessing, handling of night data as well as the number of data points used.

Regarding the pre- and postprocessing of data, two approaches were considered. In the first approach, the time series data of solar irradiance I_t is directly employed to train the models without further preprocessing. In the second approach, transmissivity $\tau_t = I_t/I_{e,t}$ is derived from observed irradiance I_t and extraterrestrial irradiance $I_{e,t}$ as described in (1). Then, the models are trained to forecast the transmissivity $\hat{\tau}_{t+j|t}$. With the extraterrestrial irradiance $I_{e,t+j}$ and $\hat{\tau}_{t+j|t}$, the irradiance forecast $\hat{I}_{t+j|t}$ is then determined.

Another hyperparameter related to the data used to train the models concerns the handling of data points at night. Here, three cases were considered: 1. include all data points from day and night, 2. only include data points between 5 am and 8 pm local time, and 3. only include data points between sunrise and sunset using condition (7). As it can be cumbersome to implement models with seasonal lags for a varying number of data points per day, the last case was not considered for seasonal models.

Table 1: Sets of hyperparameters for different forecast methods considered in search.

(a) Autoregressive integrated moving average (ARIMA) models.	
Autoregressive lags p	$0, 1, \dots, 10$
Moving average lags q	$0, 1, \dots, 10$
Differencing d	$0, 1, 2$
(b) Seasonal autoregressive integrated moving average (SARIMA) models.	
Autoregressive lags p	$0, 1, 3$
Moving average lags q	$0, 1, 3$
Seasonal autoregressive lags P	$0, 1, 2, 3$
Seasonal moving average lags Q	$0, 1, 2, 3$
Differencing d	$0, 1$
Seasonal differencing D	$0, 1$
(c) Nearest neighbor regression (NNR).	
Autoregressive lags p	$1, 2, \dots, 20$
Weight	uniform, inverse to distance
Number of neighbors k	$1, 2, \dots, 20$
Threshold ^a ε	$0.01, 0.05, 0.1, 0.5, 1$
^a Multiplied by 1360.8 W/m^2 for irradiance.	
(d) Seasonal nearest neighbor regression (SNNR).	
Autoregressive lags p	$1, 2, \dots, 11$
Seasonal autoregressive lags P	$1, 2, \dots, 7$
Weight	uniform, inverse to distance
Number of neighbors k	$1, 2, \dots, 20$
Threshold ^b ε	$0.01, 0.05, 0.1, 0.5, 1$
^b Multiplied by 1360.8 W/m^2 for irradiance.	

The last hyperparameter related to the data used concerns the number of data used for training. Here, 1, 3, 7, 14, 30, and 60 days of data were considered. For models with seasonal lags, the data used for training was assumed to include at least 14 days.

5.2.2. Model Hyperparameters

For every forecast method, the model structure can be uniquely described using model specific hyperparameters. They are not to be confused with model parameters of a trained model. For example, for SARIMA models, the number of seasonal moving average lag Q is a hyperparameter. The coefficients of the autoregressive part, ϕ_1, \dots, ϕ_p , of the trained model are model parameters. The subsets of hyperparameters that were considered in the search for all forecasting method are shown in Table 1. Note that in Table 1c depending on how the nearest neighbors are chosen, the number of neighbors k or the maximal distance to the neighbors ε is used.

5.3. Model Training

For each combination of hyperparameters defined in Section 5.2, we trained nine models, i.e., one for each location and each season described in Section 5.1. For some combinations of hyperparameters no suitable models could be found. Especially for ARIMA, no stable model could be derived for certain hyperparameters. Furthermore, for SARIMA a relatively small number of models (3.29 % of all SARIMA models) was omitted mostly due to very long training procedures that rendered them unsuitable for practical use. Still, the training procedure lead to more than 250,000 different trained forecast models.

5.4. Model Test

In the model test, the performance of the trained models shall be evaluated. Therefore, every model that was trained with for a certain combination of hyperparameters and a certain sequences of irradiance was tested by forecasting the solar irradiance of unknown test data in the corresponding subplot in Figure 4. Due to zero irradiance, data points during the night were excluded from the evaluation of the forecast accuracy using the criterion described in Section 3.2.1. For each of the data point in the test data, a 12 step ahead prediction was obtained. Using the forecast values and the known data points of the training data, the RMSE according to (8) was then calculated for every prediction step. The resulting RMSE for every prediction step, every combination of hyperparameters, location and season is then stored for the further analysis in Section 6.

Having presented the performed hyperparameter search, the interpretation of the results is performed in the next section. This interpretation aims at identifying groups of models that have a high probability of providing good forecasts.

6. Analysis

In this section, we analyze the results of the search presented in Section 5. Our goal is to draw conclusions that help to reduce the search space of future hyperparameter searches. Therefore, the search is analyzed, focusing on these forecasting methods and ranges of hyperparameters that increase the probability of finding a suitable model for unseen data. Before starting the analysis, some remarks are posed.

Remark 1. For all test data, the forecast accuracy achieved by the persistence model from Section 4.1 using transmissivity data outperformed the persistence model using irradiance data. Therefore, in the analysis the former persistence model is used as a reference.

Remark 2. The style of the box plots use throughout this work is illustrated in in Figure 5. Here, m marks the median. The box around the median contains all data from the 25th (q_1) to the 75th (q_3) percentile. The whisker at the bottom marks lowest occurring value within $q_1 - 1.5(q_3 - q_1)$ and the whisker at the top marks the highest occurring value within $q_3 + 1.5(q_3 - q_1)$. Due to numerous outliers, only every 100th outlier is shown. To assure that the forecast with the highest accuracy is considered the minimum outlier is always included.

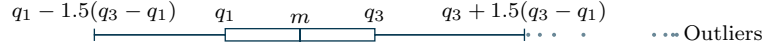


Figure 5: Box plot with median m , quantiles q_1 and q_3 , whiskers and outliers.

Remark 3. Most of the distributions of the forecast accuracy discussed in this section were similar for the nine test data sets shown in Figure 4. Therefore, the distributions were mostly merged into one plot that includes all values of the different locations. Those cases, where the distributions were not similar for the different test data sets are explicitly discussed in the corresponding subsections.

Remark 4. Throughout this paper, the forecast at the 1st, 4th and 12th prediction step were analyzed. For the 15 min sampling time considered (see Section 5.1.1), these steps correspond to a forecast 15 min, 1 h and 3 h ahead. The prediction steps were chosen to approximately analyze the evolution of the forecast accuracy for the entire prediction horizon from 15 min to 3 h.

6.1. Forecast Method

In order to reduce the search space and provide a high probability of choosing a model that accurately predicts unseen data, we first compare the forecasting methods, ARIMA and NNR along with the persistence model from Section 4.1 that acts as a reference. In Figure 6, box plots illustrating the distribution of the forecast accuracy of all models included in the search are shown.

The box plots in Figure 6 show that for predictions 15 min ahead, almost no model outperforms the persistence model. For a prediction step of 1 h this changes: some models outperform the persistence forecaster. The plot further shows that the boxes for NNR are much more compact

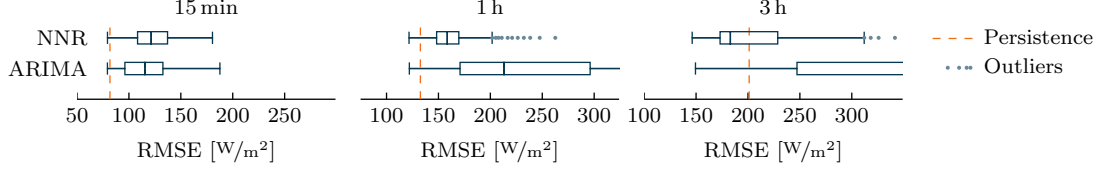


Figure 6: Forecast accuracy (mean RMSE) achieved for 15 min, 1 h and 3 h ahead predictions with ARIMA and NNR models.

than for ARIMA, i.e., the RMSE of forecasts performed with NNR varies less than the RMSE of ARIMA forecasts. This indicates a higher probability of finding a good forecast model using NNR. For predictions of 3 h ahead, the potential improvement over the persistence model is significant for all methods. As already observed for 1 h ahead predictions, the boxes for NNR are more compact. Additionally, the 25th percentile is remarkably lower for NNR. Still, the highest forecast accuracy achieved, is very alike for NNR and ARIMA for all prediction steps. In summary, the highest forecast accuracy achieved is similar for all methods, but NNR achieves significantly better results with respect to the 25th and 75th percentile as well as the median. As the probability of finding a suitable ARIMA model is much lower, we decided to use NNR forecasts. Therefore, in the following sections, it is investigated of and how the search space for NNR and SNNR, as specified in Tables 1c and 1d, can be reduced to increase the probability of finding a good forecast model. Hence, ARIMA models will not be considered further from this point on.

6.2. Preprocessing of NNR and SNNR

We are now looking into the data itself. As introduced in Section 5.2.1, models using irradiance or the normalized transmissivity values were included in the exhaustive search.

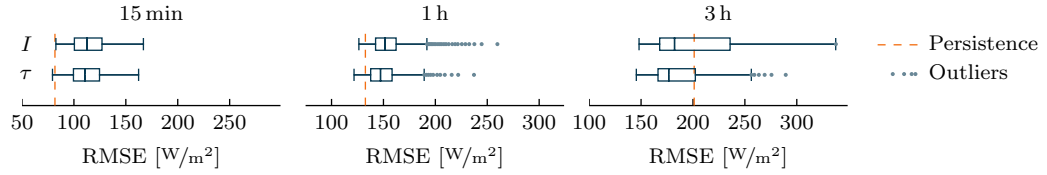


Figure 7: Forecast accuracy (mean RMSE) of NNR and SNNR using different kinds of preprocessing for all geographical positions and all seasons.

In Figure 7 the forecast accuracy of both approaches is represented using box plots. As can be observed, the box plots for 15 min forecasts are approximately equal for all test data. Also, little difference can be found for 1 h ahead predictions. For 3 h ahead predictions, the transmissivity based forecasts most of the times outperform the irradiance based forecasts, considering the highest and the median forecast accuracy. Except for the data measured in March at the NREL Clark Station during March 2–8 (see Figure 8), the best models are achieved using irradiance data. Still the lower whiskers and the medians of the box plots are approximately equal and in both cases significantly better than the persistence model.

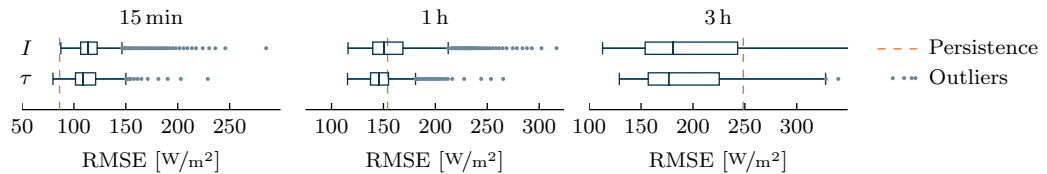


Figure 8: Forecast accuracy (mean RMSE) of NNR and SNNR using different kinds of preprocessing for NREL Clark Station during March 2–8.

The observations show that using transmissivity values yields a higher probability of finding an accurate model. Although for one test data set the model with the smallest RMSE of the 3h prediction uses irradiance instead of transmissivity, the overall distribution in this case shows no significant other difference to the probability distribution in Figure 7. As this model can be potentially hard to find, we are confident that using transmissivity values leads to a higher probability of finding a good forecast model. For this reasons, it is beneficial to use transmissivity values in the reduced search space.

6.3. Handling of Night Data of NNR and SNNR

This subsection focuses on the handling of data points at night where solar irradiance is zero. As stated in Section 5.4, data points during the night were not included in the evaluation of the forecast accuracy of the test data. However, in this analysis data points during the night were used in some cases in the historic data passed to the models to forecast future values, i.e., the reference sample. Excluding night data equally from the reference sample, i.e., the historic data, might yield to unnatural transitions between two days. Including night data in the the reference sample means that we include data points that we do not explicitly forecast as night data points are excluded in the evaluation of the forecast accuracy. As explained in Section 5.1, we used data including all data points, without data points between sunset and sunrise and without data points between 8 pm and 5 am.

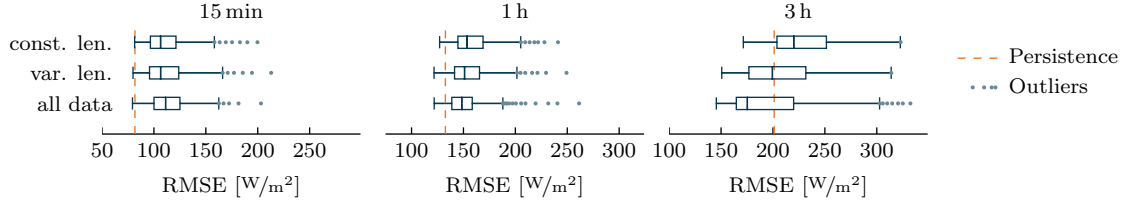


Figure 9: Forecast accuracy (mean RMSE) of NNR and SNNR using different ways to handle night data, i.e., data with constant length, variable length and all data.

In Figure 9, the forecast accuracy depending on the training data is shown. It can be observed that the forecast accuracy is similar for the 15 min forecast. For forecasts 1 h ahead, the difference between the approaches remains small. However, for forecasts 3 h ahead, using all data points for training, i.e., including night values, outperforms the other approaches. Therefore, all data points including night data are used in the reduced search space.

6.4. Size of the Reference Sample of NNR and SNNR

Now the size of the reference sample is analyzed. The reference sample is chosen such that it includes that last patterns in the historic data up to the most recent data point. A large reference sample therefore includes data that reaches further into that past than a small reference sample.

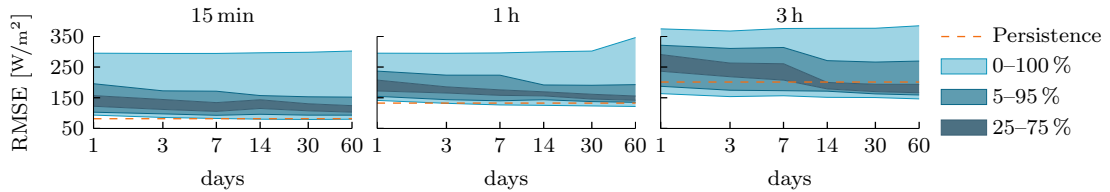


Figure 10: Forecast accuracy (mean RMSE) of NNR and SNNR using different sizes of the reference sample. Note that the x-axis is logarithmic.

In Figure 10, the achieved forecast accuracy using a reference sample of one, three and seven days as well as two weeks (14 d), three weeks (21 d), one month (30 d) and two months (60 d) are shown. The fan charts for all three prediction steps shows a small decrease of the forecast error

regarding the 25th to 75th percentile. The same can be observed for the highest forecast accuracy. Considering the largest forecast errors of each prediction step, the inverse effect can be observed. In general little difference can be observed in the forecast accuracy, when varying the size of the reference sample. However, the forecast accuracy usually increases using more data. Therefore, we decided to use a reference sample of 60 d for the reduced search space.

6.5. Autoregressive Lags of NNR and SNNR

This section focuses on the autoregressive lags, i.e., which data points of the historic data are passed as input to the forecasting model. For easier understanding, we differentiate between autoregressive lags and seasonal autoregressive lags. The former refer to continuous lags corresponding to 15 min time steps prior to the first forecast time instant. The latter refer to 24 h time steps, used to include the days prior to the forecast as introduced in Section 3.

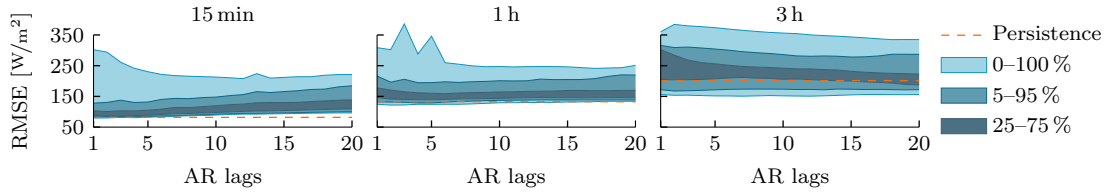


Figure 11: Forecast accuracy (mean RMSE) achieved for 15 min, 1 h and 3 h ahead predictions of NNR using different autoregressive (AR) lags.

In Figures 11, fan charts representing the forecast accuracy depending on the autoregressive lags are shown. As described in Table 1c the number of these lags is varied between 1 and 20. It can be observed for all prediction steps that the models with the highest forecast accuracy can be found for a small number of autoregressive lags. However, no clear tendency can be identified that supports choosing a particular number of autoregressive lags.

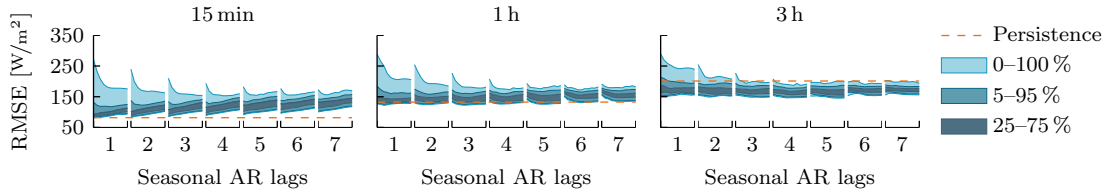


Figure 12: Forecast accuracy (mean RMSE) achieved for 15 min, 1 h and 3 h ahead predictions of SNNR using different seasonal autoregressive (AR) lags. For every seasonal AR lag, the autoregressive lags increase from 1 on the left side of the plot to 11 on the right side of the small subplot.

Figure 12 shows the RMSE for different numbers of seasonal autoregressive lags (see Section 4.3). Here, for every seasonal autoregressive lag, the number of autoregressive lags was increased from 1 (left) to 11 (right) as described in Table 1d. It can be observed in Figure 12 that for 15 min forecasts the RMSE slightly increases in most cases with the number of seasonal lags. Furthermore, for every seasonal autoregressive lag, the RMSE also increases with increasing number of non-seasonal autoregressive lags. In contrast, for the 3 h forecasts, the RMSE slightly decreases with the number of seasonal lags. It can be further observed that the 1 h and 3 h forecasts benefit from seasonal lags due to a smaller variance. This results in a higher probability of finding a good model for a higher number of seasonal lags. Unfortunately, the 15 min forecasts do not show the same effect. Based on the fact that, the 15 min forecast barely outperform the persistence model it seems reasonable focus on the improvement for larger prediction horizons. As for the 1 h and 3 h prediction step, seasonal models outperform the non-seasonal models, it seems reasonable to consider only seasonal models in the reduced search space.

6.6. Weights of NNR and SNNR

In this section, the impact of the weights are analyzed. As introduced in (18) and (20), two different kinds of weights, uniform and weights inverse to the distance to the neighbors were considered in the search. In the following, we aim to discover if applying weights inverse to the distance, i.e., emphasizing nearer neighbors can help to increase the forecast accuracy.

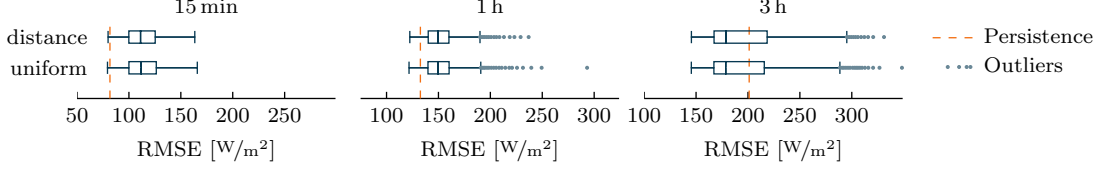


Figure 13: Forecast accuracy (mean RMSE) achieved for 15 min, 1 h and 3 h ahead predictions, using uniform weights and weights inverse to the distance of the neighbor.

As can be seen in Figure 13, the box plots regardless the prediction step hardly differ. This indicates that there is no strong correlation between forecast accuracy and the applied weights. Because of the easier implementation of uniform weights, they are chosen over weights inverse to the distance in the reduced search space.

6.7. Definition of the Neighborhood of NNR and SNNR

Having selected NNR due to its higher probability of finding an accurate model, we now analyze the impact of the neighborhood on the forecast accuracy. As introduced in Section 4.3, the neighborhood can be chosen to be a fixed number of neighbors, k , or a maximum distance, ε .

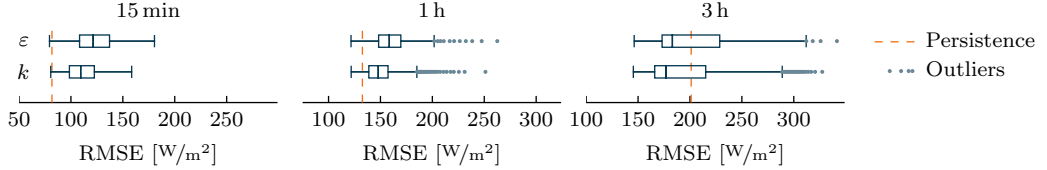


Figure 14: Forecast accuracy (mean RMSE) using a threshold ε or a fixed number of neighbors k to define the neighborhood \mathbb{K} .

As can be observed in Figure 14, the highest accuracy achieved with both hyperparameters is very alike for all prediction steps. However, the 25th and 75th percentile, the upper whisker and the median are lower for models using a fixed number of neighbors k . This indicates that the probability of choosing an accurate forecasting model, is higher when using a fixed number of neighbors k . Therefore, in the reduced search space, only models using a fixed number of neighbors k to define the neighborhood $\mathbb{K}(x_t)$, will be considered.

6.8. Number of Neighbors of NNR and SNNR

Now, the impact of the number of neighbors k is analyzed. In the search, models with up to 20 neighbors were considered.

In Figure 15, the achieved forecast accuracy of all k nearest neighbor (kNN) models included in the search are shown. It can be observed, that the forecast accuracy mainly changes using between one and five neighbors. The distribution of the RMSE becomes narrower for most cases with an increasing number of neighbors for 15 min, 1 h, and 3 h forecasts. Little improvement can be observed for the highest achieved accuracy for all prediction steps for a number of neighbors of more than ten. This improvement is less for 1 h forecasts and even less for 3 h forecast. Also, the 75th percentile if the 15 min prediction step decreases with a higher number of neighbors. In conclusion, the probability to choose a good model, increases with the number of neighbors and stays approximately equal after 10 lags. For this reason, we decided to include models using between 10 and 20 neighbors in the reduced search space.

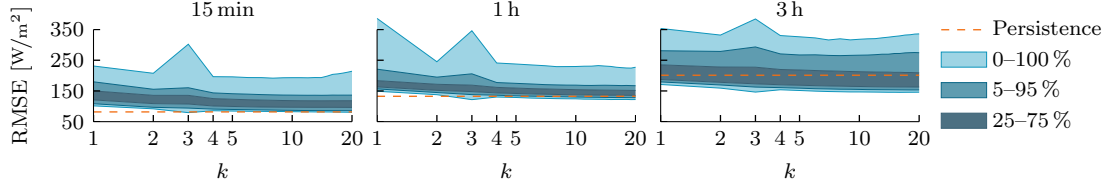


Figure 15: Forecast accuracy (mean RMSE) of NNR and SNNR using a different number of neighbors k . Note that the x-axis is logarithmic.

6.9. Summary

In summary, the following conclusions can be drawn from the analysis.

1. The probability of finding a sufficiently accurate model to forecast irradiance is much higher for NNR and SNNR than for ARIMA and SARIMA models (see Section 6.1).
2. Data pre- and postprocessing of NNR and SNNR models:
 - (a) Use transmissivity instead of irradiance (Section 6.2).
 - (b) Include night data in the reference sample (Section 6.3).
 - (c) Use data from the past 60 d in the reference sample (Section 6.4).
3. Hyperparameters of NNR and SNNR models:
 - (a) Seasonal models are beneficial (Section 6.5).
 - (b) Favor uniform weights over weights inverse to distance (Section 6.6).
 - (c) Choose the neighbors using a fixed number k instead of a maximum distance, i.e., use k nearest neighbor (kNN) regression (Section 6.7).
 - (d) Search for models with 10 to 20 neighbors (Section 6.8).

Based on these findings the hyperparameter search space, i.e., the number of potential models could be reduced from more than 250,000 to less than 1,000. The search space for suitable kNN forecasters now only includes the number of autoregressive lags, the number of seasonal autoregressive lags and the number of neighbors as shown in Table 2.

Table 2: Reduced hyperparameter search space considered in case study.

Autoregressive lags	1, 2, ..., 8
Seasonal autoregressive lags	1, 2, ..., 7
Number of neighbors k	10, 11, ..., 20

7. Case Study

After analyzing the results from the hyperparameter search we will now illustrate the use of the findings from Section 6 on a new data set. Therefore we will perform a small search using the hyperparameters from Table 2 to find kNN models that are likely to provide good forecasts.

In the case study, the data set from [29] that was obtained from a different location than the data sets used in Section 6 was employed. This data set was divided into three subsets. Each subset was then again partitioned into three subsets that were used for 1. training (first 60 d), 2. model selection (next 7 d), and 3. forecast (next 7 d). More precisely, the first part of each data subset was used to create the reference sample which is equivalent to the training data. The second part was used to test the trained models and find the most accurate model, i.e., the model with the lowest average RMSE. This model is then selected and used to forecast values from the third part

of each data subset, shown in Figure 16. This way, out of sample forecasts [19], i.e., forecast on a different data subset than the one used to select the model, could be obtained. The most recent week used to forecast unseen data with different climatic situations (sunny, foggy and cloudy) is shown in Figure 16. The week before that was used for model selection and the 60 d before that as reference sample.

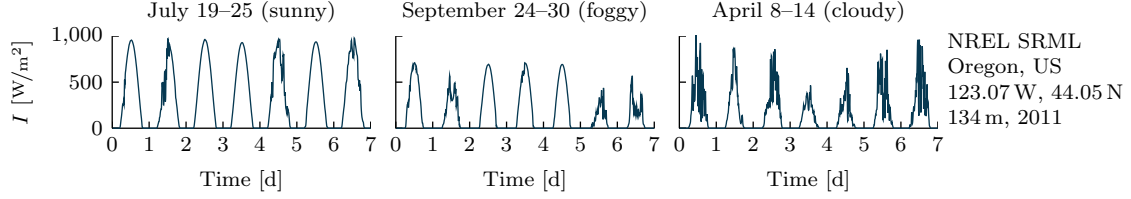


Figure 16: Three weeks of solar irradiance data used to assess the forecasts of the identified models.

The parameters of the resulting kNN models that were identified in the model selection and used to forecast data of the sunny, foggy and cloudy week are shown in Table 3. In the model selection and forecast of these models we also attempted to update the reference sample after each prediction by adding the last measured value. However, the improvement that could be achieved with this showed in a decrease in the RMSE of less than 4 W/m^2 for all prediction steps and models. Therefore, the update the reference sample was not further considered in the case study.

Table 3: Identified hyperparameters for different weather conditions.

	Jul. 19–25 (sunny)	Sep. 24–30 (foggy)	Apr. 8–14 (cloudy)
Autoregressive lags	10	2	1
Seasonal autoregressive lags	1	1	1
Number of neighbors k	10	12	10

The results of the case study in the form of the forecast RMSE for the data used for model selection and for forecast is shown in Figure 17. Note that the RMSE of the data used for model selection is low, because the selection was based on the average value of exactly this RMSE. It is included in Figure 17 to provide a reference for the RMSE of the forecast on the unseen data. For the sunny week and the cloudy week, the RMSE of the model selection is lower than for the forecast. In contrast, due to very low irradiance the foggy week shows a higher RMSE for the model selection and a lower RMSE for the forecast stage. Furthermore, the results in Figure 17 show that the forecast accuracy of the selected models is usually below the persistence model. Especially for prediction horizons of more than 2 h all kNN models outperform the persistence models. It can be further observed that the gap between persistence model and the kNN is greatest for the sunny week. Also, the gap between persistence and the kNN model is greater for the cloudy than for the foggy week.

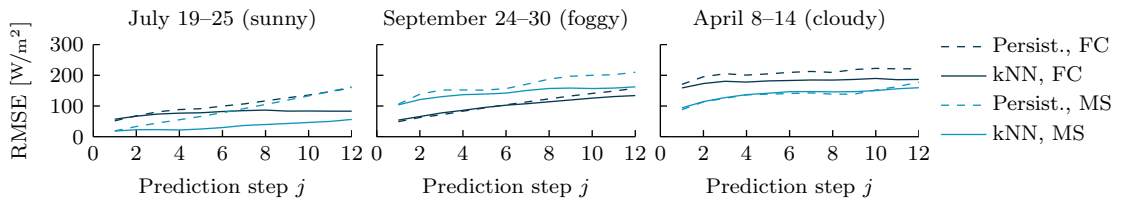


Figure 17: RMSE of model selection (MS) and forecast (FC) of persistence model and most promising kNN models for different climatic situations. The kNN models were selected based on the lowest average RMSE during MS and then used to obtain the RMSE of the FC stage.

In conclusion, the results of the case study show that kNN models that are likely to provide good forecasts can be found using the reduced parameters space. kNN without any exogenous inputs

provides a forecasting method that can be implemented with reasonable effort and a satisfying forecast accuracy.

8. Conclusion

8.1. Summary

The comparison of ARIMA and NNR for short term solar forecasts led us to choose NNR as the forecasting method providing higher probability of finding a good forecasting model. Based on this comparison, we were able to derived a reduced search space of models that are likely to provide a good forecast on unseen data. In a case study, this search space was used to find forecast models that were able to significantly outperform a persistence forecaster.

8.2. Future Work

Future work concerns an extension of the current approach to exogenous data and comparison to the forecast accuracy achieved. Also, using other artificial intelligence based methods, e.g., neural networks and support vector regression in combination with other optimization techniques, e.g., random search [30], planed to be investigated. The presented results, also indicate that nearest neighbor regression could provide accurate forecasts for larger prediction horizons than 3 h. Additionally, the quality in the estimation of forecast probability distributions shall be investigated for the different forecast models.

Acknowledgements

We would like to thank Jonas Hagemann for fruitful discussions and insights. Also, we wish to thank Ajay Kumar Sampathirao and Steffen Hofmann for proofreading and helpful discussions.

References

- [1] Renewables 2017 global status report, Tech. rep., REN21 (2017).
- [2] P. Denholm, M. Hand, Grid flexibility and storage required to achieve very high penetration of variable renewable electricity, *Energy Policy* 39 (3) (2011) 1817–1830.
- [3] S. R. West, D. Rowe, S. Sayeef, A. Berry, Short-term irradiance forecasting using skycams: Motivation and development, *Solar Energy* 110 (2014) 188–207.
- [4] H. T. Pedro, C. F. Coimbra, Assessment of forecasting techniques for solar power production with no exogenous inputs, *Solar Energy* 86 (7) (2012) 2017–2028.
- [5] H. T. Pedro, C. F. Coimbra, Nearest-neighbor methodology for prediction of intra-hour global horizontal and direct normal irradiances, *Renewable Energy* 80 (2015) 770–782.
- [6] J. Shi, W.-J. Lee, Y. Liu, Y. Yang, P. Wang, Forecasting power output of photovoltaic systems based on weather classification and support vector machines, *IEEE Transactions on Industry Applications* 48 (3) (2012) 1064–1069.
- [7] P. Bacher, H. Madsen, H. A. Nielsen, Online short-term solar power forecasting, *Solar Energy* 83 (10) (2009) 1772–1783.
- [8] J. Zeng, W. Qiao, Short-term solar power prediction using a support vector machine, *Renewable Energy* 52 (2013) 118–127.
- [9] G. Reikard, Predicting solar radiation at high resolutions: A comparison of time series forecasts, *Solar Energy* 83 (3) (2009) 342–349.
- [10] A. Sfetsos, A. Coonick, Univariate and multivariate forecasting of hourly solar radiation with artificial intelligence techniques, *Solar Energy* 68 (2) (2000) 169–178.

- [11] A. Mellit, A. M. Pavan, A 24-h forecast of solar irradiance using artificial neural network: Application for performance prediction of a grid-connected PV plant at Trieste, Italy, *Solar Energy* 84 (5) (2010) 807–821.
- [12] EPEX SPOT SE, 15-minute intraday call auction - the new meeting point for the German market, accessed Apr. 24, 2018 (2016).
URL <https://www.epexspot.com/document/29113/15-Minute%20Intraday%20Call%20Auction>
- [13] ISO 9488:1999, Solar Energy – Vocabulary, International Organization for Standardization, Geneva, CH, 1999.
- [14] W. B. Stine, R. W. Harrigan, *Solar Energy Systems Design*, John Wiley and Sons, Inc., 1986.
- [15] ARM, Atmospheric radiation measurement climate research facility, surface meteorology system (MET), Eastern North Atlantic Facility ARM Data Archive: Oak Ridge, USAccessed Jul. 14, 2011.
- [16] I. Reda, A. Andreas, Solar position algorithm for solar radiation applications, *Solar energy* 76 (5) (2004) 577–589.
- [17] V. Quaschnig, *Regenerative Energiesysteme*, München, Hanser, 2009.
- [18] M. J. Reno, C. W. Hansen, J. S. Stein, Global horizontal irradiance clear sky models: Implementation and analysis, Tech. Rep. SAND2012-2389, Sandia National Laboratories (2012).
- [19] C. Chatfield, *Time-Series Forecasting*, CRC Press, 2000.
- [20] G. Bontempi, S. B. Taieb, Y.-A. Le Borgne, Machine learning strategies for time series forecasting, in: *European Business Intelligence Summer School*, Springer, 2012, pp. 62–77.
- [21] J. H. Meeus, *Astronomical algorithms*, Willmann-Bell, Inc., 1991.
- [22] A. Sfetsos, A novel approach for the forecasting of mean hourly wind speed time series, *Renewable energy* 27 (2) (2002) 163–174.
- [23] G. E. P. Box, G. M. Jenkins, G. C. Reinsel, *Time Series Analysis - Forecasting and Control*, Prentice- Hall, Inc., 1994.
- [24] The MathWorks, Inc., *Matlab and econometrics toolbox release 2015b*, Massachusetts, United States.
- [25] N. S. Altman, An introduction to kernel and nearest-neighbor nonparametric regression, *The American Statistician* 46 (3) (1992) 175–185.
- [26] D. Lin, *Statistical learning toolbox* (2006).
- [27] A. Andreas, T. Stoffel, Nevada power: Clark station; Las Vegas, Nevada, US (data), Tech. Rep. DA-5500-56508, National Renewable Energy Lab. (NREL), Golden, US (2006).
- [28] A. Andreas, T. Stoffel, NREL solar radiation research laboratory (SRRL): Baseline measurement system (BMS); Golden, Colorado, US (data), Tech. Rep. DA-5500-56488, National Renewable Energy Lab. (NREL), Golden, US (1981).
- [29] F. Vignola, A. Andreas, University of Oregon: GPS-based precipitable water vapor (PWV), Tech. Rep. DA-5500-64452, National Renewable Energy Lab. (NREL), Golden, US (2013).
- [30] J. Bergstra, Y. Bengio, Random search for hyper-parameter optimization, *Journal of Machine Learning Research* 13 (2012) 281–305.